

**COMPUTED POTENTIAL ENERGY SURFACES
FOR CHEMICAL REACTIONS**

*AMES GRANT
10-25-CR
158859
428*

Semi-Annual Report
for
Cooperative Agreement NCC2-478

for the period
January 1, 1988 - June 30, 1988

Submitted to

National Aeronautics and Space Administration
Ames Research Center
Moffett Field, California 94035

Computational Chemistry Branch
Dr. David Cooper, Chief and Technical Monitor

Thermosciences Division
Dr. Jim Arnold, Chief

Prepared by

ELORET INSTITUTE
1178 Maraschino Drive
Sunnyvale, CA 94087
Phone: 408 730-8422 and 415 493-4710
Telefax: 408 730-1441

K. Heinemann, President and Grant Administrator
Stephen P. Walch, Principal Investigator

(NASA-CR-183168) COMPUTED POTENTIAL ENERGY
SURFACES FOR CHEMICAL REACTIONS Semiannual
Report, 1 Jan. - 30 Jun. 1988 (Eloret
ccip.) 42 p

N88-29893

CSCI 07D

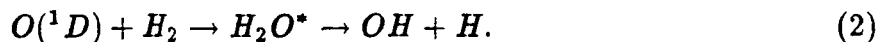
Unclas
G3/25 0158859

In the first year of the grant, potential energy surfaces (PES's) have been calculated for a number of reactions. The reactions currently under study are relevant to the design of the SCRAM jet engine for the NASP. Two hydrogen/oxygen reactions have been studied. The first reaction,



is the most important chain propagation reaction in combustion. Although there have been previous studies of reaction (1), they focused on the $H + O_2$ region of the surface and a detailed examination of the $OH + O$ region was needed. This latter region of the surface is complex, because chemical bonding and long range electrostatic forces compete, leading to an $OH - O$ minimum at large OO distances ($\approx 6.0 a_0$) followed by a saddle point before the HOO well. Approximately 150 points have been obtained which characterize the minimum energy path (MEP) for the entire PES. Additional points will be computed to characterize the hydrogen atom transfer process. In collaboration with Ron Duchovic (Eloret Institute), the complete set of points will be used to generate a global PES suitable for dynamical studies. A more detailed discussion of this work is given in ref. 2.

An additional hydrogen/oxygen reaction which has been studied is the reaction



The reason for studying this system is that $O(^1D)$ formed by photolysis of O_2 could be used as a means of initiating combustion at lower temperatures in the SCRAM jet engine. As discussed in the semiannual report for the first six months of this grant, both the vibrational energy distribution in the OH product and the OD/OH ratio when $O(^1D)$ is reacted with HD seem to depend critically on the long range behavior of the potential. The new, more accurate, potential energy surface may explain discrepancies between

previous dynamical studies and experiment. A more detailed discussion of this work is given in ref. 3.

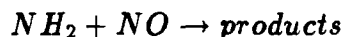
Another important group of reactions for design of the SCRAM jet are three body recombination reactions. As a start in this area, calculations were carried out for the reactions



and



since the combination of eqns (3)-(4) constitutes a mechanism for H atom recombination with N_2 acting as a third body. HN_2 is also a very important intermediate in Thermal DeNO_x processes. Specifically, addition of NH_3 leads to substantial NO_x reduction in hydrocarbon combustion. The key step here is thought to be



where the expected products are $HN_2 + OH$ and $N_2 + H_2O$. The observed branching ratio varies from study to study and while there is no direct evidence that HN_2 is formed, OH is observed but H atoms are not. The presence of an HN_2 intermediate is also implicated indirectly by modeling studies which require chain propagation steps producing OH in order to explain the DeNO_x process.

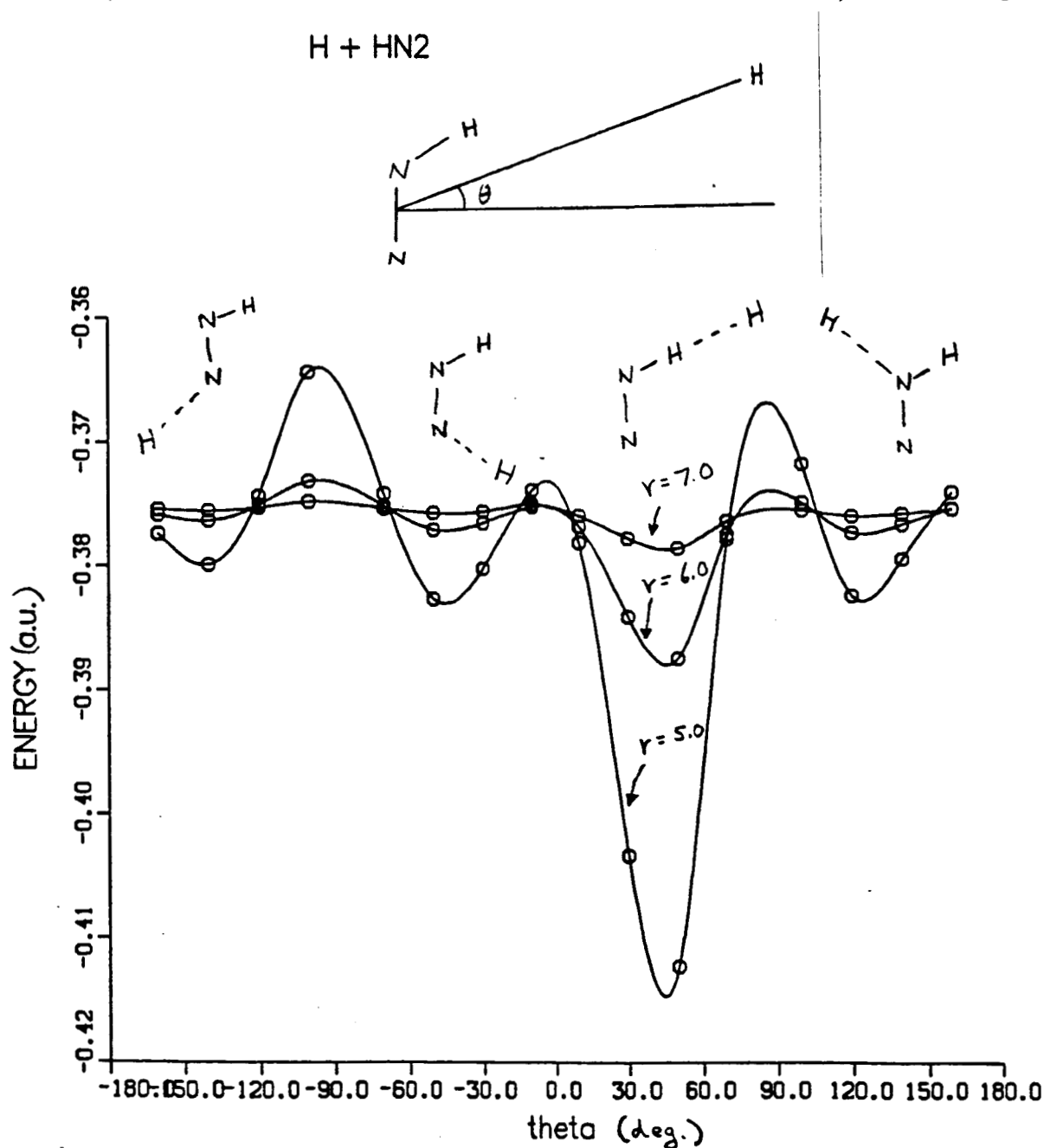
A key factor, currently undetermined, is the lifetime of the HN_2 species. The potential for dissociation of HN_2 has a shallow well ≈ 3 kcal/mole above the $H + N_2$ asymptote and separated from that asymptote by a barrier. The dissociation process is primarily controlled by quantum mechanical tunneling. Enough points on the HN_2 dissociation potential have been obtained to characterize the MEP. Approximate calculations (one-dimensional tunneling through an Eckart barrier) have been carried out to determine

the rate of dissociation via tunneling. Additional electronic structure calculations with larger basis sets were carried out in collaboration with Celeste Rohlif (Sandia National Laboratories, Livermore) to assess the accuracy of the computed potential. The larger basis set calculations indicate that the PES is converged to $\approx \pm 1.0$ kcal/mol. Based on this and the tunneling calculations the lifetime of HN_2 is estimated to be less than 10^{-8} sec. This is much shorter than values of about 10^{-4} sec which would fit current models of thermal de- NO_x processes. This result suggests that there may be other important processes not included in the current models. A more detailed discussion of this work will be found in ref. 4.

Part of the potential for reaction (4) is shown in Fig. 1. Here the geometry of the HN_2 molecule is fixed at close to the computed equilibrium geometry and the distance between the second H and the center of mass of the N_2 as well as the polar angle are varied. From Fig. 1 it is seen that there are three channels which lead to stable minima (cis and trans HNNH and H_2NN) and a fourth abstraction channel which leads to $\text{N}_2 + \text{H}_2$. These results indicate that HN_2 is a very reactive species which is consistent with the short computed lifetime. At the current time it appears that the lifetime of HN_2 is too short for H atom abstraction from this species to contribute significantly to the $\text{H} + \text{H} + \text{N}_2$ three body recombination process; i.e. the dominant process may involve a different mechanism such as stabilization of a metastable H_2 species. Study of the latter process would require regions of the surface which were not considered in the present study; although, the HN_2 potential discussed above would be a good starting point.

NO will be an important species in the SCRAM jet engine. Since H atoms will also be present the potential surfaces for HNO are important. Currently studies are underway to characterize the lowest three surfaces ($^1\text{A}'$, $^3\text{A}''$, and $^1\text{A}''$) of HNO . Fig. 2 shows the potential for H atom addition to the N end of NO . The lowest surface, which involves addition to the radical orbital of NO , has no barrier, while the other two surfaces, which involve addition to the π bond of NO , have barriers. The HNO region of these three sur-

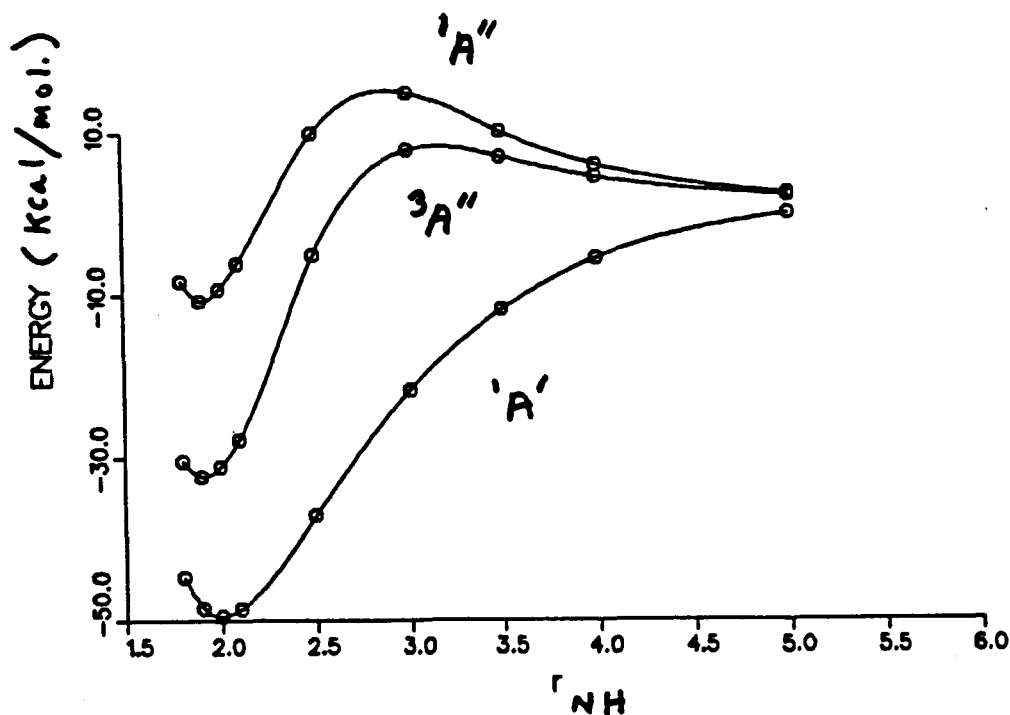
Fig. 1. The potential for the interaction of an H atom with HN_2 . The HN_2 geometry is fixed at near the computed equilibrium geometry and the energy is shown as a function of i) the distance between H and the center of mass of N_2 and ii) the polar angle (θ).



faces has been characterized. The computed geometries for the $^1\text{A}'$ ground state and $^1\text{A}''$ excited state as well as the computed excitation energy are in good agreement with experiment. Calculations are also underway to examine the NOH region of the same three surfaces. These results will be combined with calculations in collaboration with

Celeste Rohlffing and Carl Melius at Sandia National Laboratory, Livermore on the O + NH and N + OH regions of the potential to produce a global potential for HNO.

Fig. 2. The energy as a function of r_{NH} along the minimum energy path for H atom addition to the N end of NO for the lowest $^1A'$, $^3A''$, and $^1A''$ surfaces of HNO.



In the next year a number of projects will be completed. As mentioned above, additional points will be obtained for reaction (1). Studies on HNO will also be completed in collaboration with scientists at Sandia National Laboratory, Livermore. In collaboration with Ron Duchovic (Eloret), global representations of these potential surfaces will be constructed, and dynamical studies will be carried out using both statistical methods (RRKM theory and transition state theory) and classical trajectories. Further, quantum dynamical studies will be completed in collaboration with Dave Schwenke (Eloret). Finally, new studies using the improved $O(^1D) + H_2$ potential energy surface will be carried out by George Schatz (Northwestern University).

Current Publications

1. Theoretical Studies of the Potential Surface for the $F + H_2 \rightarrow HF + H$ Reaction., C.W. Bauschlicher, Jr, S.P. Walch, S.R. Langhoff, P.R. Taylor, and R.L. Jaffe, J. Chem. Phys., **88**, 1743(1988).
2. Theoretical Characterization of the Minimum Energy Path for the Reaction $H + O_2 \rightarrow HO_2^* \rightarrow HO + O$, S.P. Walch, C.M. Rohlfiing, C.F. Melius, and C.W. Bauschlicher, Jr., J. Chem. Phys., **88**, 6273(1988).
3. An Improved Long Range Potential for $O(^1D) + H_2$, S.P. Walch and L.B. Harding, J. Chem. Phys., **88**, 7653(1988).
4. Theoretical Characterization of the Minimum Energy Path for H Atom Addition to N_2 , S.P. Walch and R.J. Duchovic, J. Chem. Phys., manuscript in preparation.

**Theoretical Characterization of the Minimum Energy Path
for Hydrogen Atom Addition to N₂
Implications for the Unimolecular Lifetime of HN₂**

Stephen P. Walch^a and Ronald J. Duchovic^a

ELORET Institute
Sunnyvale, CA 94087 USA

and

Celeste McMichael Rohlfing
Sandia National Laboratory
Livermore, CA 94550 USA

Abstract

The minimum energy path (MEP) for the addition of a hydrogen atom to N₂ is characterized in CASSCF/CCI calculations using the [4s3p2d1f/3s2p1d] basis set, with additional single point calculations at the stationary points of the potential energy surface using the [5s4p3d2f/4s3p2d] basis set. These calculations represent the most extensive set of *ab initio* calculations completed to date, yielding a zero-point corrected barrier for HN₂ dissociation of ≈ 8.5 kcal mol⁻¹. The lifetime of the HN₂ species is estimated from the calculated geometries and energetics using both conventional Transition State Theory and a method which utilizes an Eckart barrier to compute one-dimensional quantum mechanical tunneling effects. This study concludes that the lifetime of the HN₂ species is very short, greatly limiting its role in both termolecular recombination reactions and combustion processes.

^aMailing Address: NASA Ames Research Center, Moffett Field, CA 94035 USA

I. Introduction

The proposed National Aerospace Plane will be powered by an air-breathing, hydrogen-burning, supersonic ramjet (SCRAMjet) engine. The supersonic flow in the combustor and nozzle regions of the SCRAMjet will allow only very short residence times for the reactants, and consequently, accurate knowledge of the finite rates of reaction is critical to design of the engine. The rates of recombination processes are of special interest since these reactions can lead to considerable heat evolution and their rates, under conditions of high temperature and supersonic flow, are not well-known experimentally. One such reaction which is expected to be important under these conditions is the recombination of two hydrogen atoms in the presence of N_2 :



The various mechanisms proposed to describe three-body recombination processes involve the formation of a metastable species. For reaction (1), the expected metastable species is either H_2^* (vibrationally-rotationally excited H_2), which can be stabilized by subsequent collisions with N_2 , or an HN_2 species, which can then react with a hydrogen atom to yield bound H_2 :



Calculations characterizing reaction (2) will be the subject of a future publication. We simply note here that these calculations indicate there is no barrier to reaction (2). However, in addition to the region of the potential energy surface which controls the abstraction process, there are three additional regions of the surface which lead

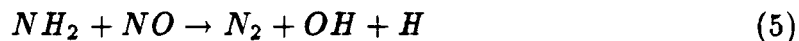
to stable H_2N_2 species (cis HNNH , trans HNNH , and H_2NN). While the HN_2 species has not been observed experimentally, indirect evidence for its existence has been obtained from experimental studies of the reaction:



This reaction constitutes one possible step in the complicated mechanisms which describe the fundamental chemistry of nitric oxide both in the troposphere¹ and in combustion²⁻⁵ processes. As a result, it has been studied extensively with a variety of experimental techniques over a range of temperatures and pressures. Early studies⁶⁻¹⁵ suggested that the major pathway is the reaction:



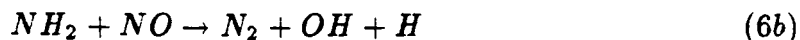
Vibrationally excited H_2O and small amounts of the NH_2NO complex were observed along with a negative temperature dependence of the rate coefficient. Gehring et al.¹¹ did entertain the possibility of an alternate pathway:



However, a careful search using ESR techniques failed to identify any measurable quantity of hydrogen atoms.

In subsequent studies¹⁶⁻²⁹, investigators considered a reaction mechanism which includes three possible product channels:





Each of these experiments attempted to determine the rate coefficient of the $NH_2 + NO$ reaction as well as the major pathway of this reaction. The results of the studies are far from consistent. Stief et al.¹⁸ did not observe OH radicals, suggesting that the branching ratio for the formation of OH radicals is substantially less than 0.22 at 298 K. Further, both ESR techniques and Lyman-alpha fluorescence could not detect the production of hydrogen atoms. Hall et al.²⁶, using infrared absorption at 298 K, reported that the OH channels account for only $13 \pm 2\%$ of the reaction, while Dolson²⁹ attributed 15% of the reaction to OH radical production at 300 K. In contrast, Silver and Kolb¹⁷ determined that approximately 40% of the $NH_2 + NO$ reaction produced OH radicals over a temperature range of 294 – 1215 K, although, at room temperature, they did not observe hydrogen atoms. Andresen et al.²⁰, operating an isothermal flow reactor at temperatures ranging from 300 K to 1150 K, reported that the OH branching ratio is greater than 0.65 but that hydrogen atoms were not detected for temperatures from 300 K to 900 K. Finally, Kimball-Linne and Hanson²⁷ observed a branching ratio for OH radical formation of 0.48 at 1050 K and a ratio of greater than 0.80 at 1400 K.

Despite the wide variation in the reported branching ratios for OH radical formation, the experimental results consistently indicate, over a range of temperatures, that hydrogen atoms are not produced. In light of equation (6), the observation of OH radicals without the production of hydrogen atoms indirectly argues for the existence of the rather exotic species, HN_2 . However, none of the experimental studies have directly detected the presence of HN_2 . Additional arguments for the existence of the HN_2 species have been made by researchers constructing kinetic

models of combustion processes^{3,4}. These models include several reactions of HN_2 as critical steps and require that this species possess a lifetime which is long enough to allow its participation in these reactions.

There have been a number of previous *ab initio* studies³⁰⁻³⁵ of the reaction:



characterizing the geometry and energetics of the reactant, transition state, and products. The most recent of these earlier studies, the work of Curtiss et al.³⁵, concisely summarizes the methodologies and basis sets used in these investigations. At the SCF level of theory, the dissociation energy of HN_2 to $\text{H} + \text{N}_2$ was determined to have a value varying from $-9.6 \text{ kcal mol}^{-1}$ to $+13.6 \text{ kcal mol}^{-1}$ with a barrier to dissociation (before zero-point energy corrections) of $22.6 \text{ kcal mol}^{-1}$. The first two studies which treated electron correlation failed to resolve these early discrepancies. Vasudevan et al.³¹ estimated the dissociation energy of HN_2 to $\text{H} + \text{N}_2$ at $3.8 - 4.4 \text{ kcal mol}^{-1}$ with an barrier height of $10 - 15 \text{ kcal mol}^{-1}$. Casewit and Goddard³⁴ concluded that the dissociation energy is $-20.0 \text{ kcal mol}^{-1}$ but did not reinvestigate the barrier height. In their study, Curtiss et al.³⁵ utilized third-order and fourth-order Møller-Plesset perturbation theory (MP3/MP4) to account for electron correlation effects and a double zeta basis set which included polarization functions (6-31G**) to compute a dissociation energy of $-14.4 \text{ kcal mol}^{-1}$ and a barrier of $10.5 \text{ kcal mol}^{-1}$. Using their calculated geometries and energetics in conjunction with Conventional Transition State Theory (including an estimate of quantal tunneling), Curtiss et al. then determined an approximate lifetime for the HN_2 radical.

While Møller-Plesset perturbation theory techniques work well in regions which

are well-described by single configuration SCF wavefunctions, difficulties do arise when bonds are stretched and when multiply-bonded systems such as N_2 are involved. Given the possible importance of the HN_2 species in a number of chemical systems, we decided to carry out an extensive calculation of the potential energy surface for the addition of hydrogen atom to N_2 , using Complete Active Space/externally Contracted CI wavefunctions (CASSCF/CCI)³⁶ along with good quality Atomic Natural Orbital (ANO) basis sets³⁷. We have utilized these new calculations to study the lifetime of the HN_2 radical, using both Conventional Transition State Theory³⁸ and the formalism of W. H. Miller³⁹ which utilizes an Eckart Barrier to estimate one-dimensional quantum mechanical tunneling.

The *ab initio* computational method is discussed in Section II. with the results of these calculations presented in Section III. Section IV. then discusses the dynamical methods used in this study along with an estimate of the lifetime of the HN_2 species. Finally, Section V. summarizes our conclusions.

II. Ab Initio Computational Details

Using a localized orbital description, the ground state of HN_2 is represented by equation (8):

In equation (8), one NN π bond has been broken and an NH σ bond has been formed. Since the two bonds (one formed and one broken) are of about equal strength, a significant barrier is expected to occur in the entrance channel. Consequently, the

potential energy surface for hydrogen atom addition to N_2 has two stationary points, a saddle point for $R_{NH} \approx 2.7 a_0$ and a minimum for $R_{NH} \approx 2.0 a_0$.

ANO basis sets³⁷ are used in the present study. Since these basis sets are optimal for describing the atomic correlation effects, they have very small basis set superposition errors, but they are sufficiently flexible to be used in molecular calculations at both the SCF and CI levels. The N and H basis sets are $(13s8p6d4f)/[4s3p2d1f]$ and $(8s6p4d)/[3s2p1d]$, respectively, and are described in detail in reference 37. While these basis sets were expected to describe the molecular potential energy curves accurately, additional calculations were completed with larger N, $(13s8p6d4f)/[5s4p3d2f]$, and H, $(8s6p4d)/[4s3p2d]$, basis sets, in which the additional contracted functions correspond to higher energy atomic natural orbitals. These additional calculations were carried out at both the stationary point geometries determined with the smaller basis sets, and the $H + N_2$ geometry.

Table I. describes the qualitative character of the CASSCF orbitals for both $H + N_2$ and HN_2 . The $1a'$ and $2a'$ orbitals correspond to the N $1s$ orbitals, which were not correlated in these calculations, while the $3a'$ and $4a'$ orbitals correspond to the N $2s$ orbitals. The $5a'$ and $9a'$ orbitals are the natural orbitals of the N_2 σ bond pair. At large R_{NH} , the $6a'$ orbital corresponds to the N_2 $1\pi_u$ orbital, the $7a'$ orbital to the H $1s$ orbital, and the $8a'$ orbital to the N_2 $1\pi_g$ orbital. At shorter R_{NH} , there is considerable mixing of the orbitals which are appropriate in the limit of large R_{NH} . Near the HN_2 minimum, the $6a'$ orbital corresponds to the N_2 $1\pi_u + H$ $1s$, the $7a'$ orbital to N_2 $1\pi_g + H$ $1s$, and the $8a'$ orbital to N_2 $1\pi_g - H$ $1s$.

Orbitals $4a'$ through $9a'$, and the $1a''$ and $2a''$ orbitals were active in the CASSCF calculations. This CASSCF treatment in six active a' and two active a'' orbitals is denoted as a (62) CASSCF. The inclusion of the $4a'$ orbital in the active space was not conceptually necessary based on equation (8), but it was found that the larger

(62) active space led to better CASSCF convergence, even though the CASSCF wavefunction of this orbital contained no configurations with CI coefficients greater than 0.05. In the CCI calculations, all but the N 1s electrons (the 1a' and 2a' orbitals) were correlated. The CCI list of reference configurations was obtained by selecting the unique configurations from the H + N₂ region, the saddle point region, and the HN₂ minimum region whose CI coefficients in the CASSCF wavefunction were greater than 0.05. The multireference analogue of Davidson's correction⁴⁰ was computed to estimate the importance of higher-order excitations. This correction to the CCI energy is given by

$$Q = \Delta E(1 - C_0^2)/C_0^2 \quad (9)$$

where ΔE is the CI energy minus the reference energy, and C_0^2 is the sum of the squares of the coefficients of the reference configurations in the CI wavefunction.

The calculations using the smaller basis set were carried out on the NASA Ames Cray X-MP/48. These calculations used the MOLECULE - SWEDEN^{41,42} system of programs. The calculations using the larger basis set were carried out at Sandia National Laboratory on a Cray X-MP/416.

III. Ab Initio Results

Table II. lists the parameters of the N₂ molecular potential energy surface which were computed with the [4s3p2d1f] and the [5s4p3d2f] basis sets. In order to be consistent with the HN₂ analysis, the diatomic calculations included the N 2p derived orbitals and the N₂ 2 σ_u orbital in the active space. The CCI reference list was larger than in the HN₂ case, consisting of all the configurations generated from the N 2p derived levels. As the Table indicates, the smaller basis set yields values for

R_e , ω_e , and D_0 which differ from the corresponding experimental⁴³ quantities by 0.022 a_0 , 73 cm^{-1} , and 13 kcal mol^{-1} (based on a Dunham analysis of a quadratic fit near R_e). The value of D_0 computed in this work differs from that previously calculated with a segmented basis set of the same size⁴⁴ by 0.5 kcal mol^{-1} . This earlier study⁴⁴ concluded that the error resulting from the externally contracted CI procedure is expected to be only 0.16 kcal mol^{-1} (determined by comparing CCI + Q and SDCI + Q results). Consequently, limitations in the basis set itself are responsible for the remaining difference between the value of D_0 calculated in this work and the experimental value.

The value of ω_e for N_2 computed in this study is 248 cm^{-1} smaller than that obtained from the MP3/6-31G** calculations of Curtiss et al.³⁵, and underestimates the experimental harmonic frequency by approximately 3.1% compared with an overestimate of approximately 7.4% by the Møller-Plesset perturbation theory calculations. Curtiss and co-workers suggested that the discrepancy between their calculated N_2 frequency and the experimental value is a consequence of limitations in the 6-31G** basis set. This conclusion is consistent with the earlier work of Siegbahn³⁶. Additionally, as Bartlett and Purvis⁴⁵, and more recently, Laidig et al.⁴⁶ have discussed, the multiply-bonded N_2 system cannot be represented satisfactorily using only a single-reference, many-body perturbation theory (MBPT) technique. Consequently, it appears that limitations in both the basis set and the computational methodology have contributed to the anomalous N_2 frequency reported by Curtiss and co-workers. It should be noted, however, that even the CASSCF/CCI calculations reported in this work, utilizing a good quality ANO basis set, fail to represent precisely the experimental values of both D_0 and the harmonic stretching frequency of the N_2 triple bond system.

The larger basis set, [5s4p3d2f], reduces these errors to

The first three columns of Table III. summarize the computed geometries and harmonic vibrational frequencies at the stationary points of the $\text{H} + \text{N}_2$ potential energy surface (using the $[4s3p2d1f/3s2p1d]$ basis set). The values of R_{NN} and ω_2 at the $\text{H} + \text{N}_2$ minimum were derived from supermolecule calculations and are very similar to the values of R_e and ω_e obtained for N_2 with the $[4s3p2d1f]$ basis set (see Table II). These results differ because the diatomic calculations used all possible reference configurations from the active space to estimate electron correlation, while the supermolecule calculations utilized a set of selected reference configurations from the same active space. Energetically, the HN_2 species lies $3.01 \text{ kcal mol}^{-1}$ above the $\text{H} + \text{N}_2$ asymptote, while the saddle point for hydrogen atom addition is $15.16 \text{ kcal mol}^{-1}$ above $\text{H} + \text{N}_2$. Thus, there is a barrier of $12.15 \text{ kcal mol}^{-1}$ to the dissociation of HN_2 to $\text{H} + \text{N}_2$. The addition of zero-point energy corrections reduces this barrier to $8.49 \text{ kcal mol}^{-1}$. Single-point calculations with the $[5s4p3d2f/4s3p2d]$ basis set (at the stationary point geometries determined with the $[4s3p2d1f/3s2p1d]$ basis set) indicate that the HN_2 species and the saddle point are $3.73 \text{ kcal mol}^{-1}$ and $15.01 \text{ kcal mol}^{-1}$, respectively, above the $\text{H} + \text{N}_2$ asymptote, thus yielding a dissociation barrier for HN_2 of $11.28 \text{ kcal mol}^{-1}$.

The harmonic vibrational frequencies of Table III. are based on normal mode analyses performed at the stationary points of the $\text{H} + \text{N}_2$ potential energy surface. ω_1 , ω_2 , and ω_3 are the frequencies of the normal modes which correspond principally to the NH stretching motion, the NN stretching motion, and the HNN bending motion. The value of ω_2 decreases from 2303 cm^{-1} at the $\text{H} + \text{N}_2$ asymptote, to 2072 cm^{-1} at the $\text{H}-\text{N}_2$ saddle point, and finally, to 1583 cm^{-1} at the HN_2 minimum. Simultaneously, the value of ω_1 (the frequency which essentially corresponds to the reaction coordinate for hydrogen atom addition to N_2), changes from an imaginary value ($1662i \text{ cm}^{-1}$) at the $\text{H}-\text{N}_2$ saddle point to a value of 2744

cm^{-1} at the HN_2 minimum. Finally, the value of ω_3 increases from 771 cm^{-1} at the $\text{H}-\text{N}_2$ saddle point to 1070 cm^{-1} at the HN_2 minimum. These changes are consistent with the breaking of an NN π bond and simultaneous formation of an NH σ bond as the HN_2 species forms.

Table III. also compares the results obtained in the present study at the stationary points of the $\text{H} + \text{N}_2$ surface with those reported by Curtiss et al.³⁵. The current calculations suggest that the HN_2 species is energetically more stable than predicted by the earlier work, lying only $3.01 \text{ kcal mol}^{-1}$ rather than previously calculated $14.4 \text{ kcal mol}^{-1}$ above the $\text{H} + \text{N}_2$ asymptote. In addition, the barrier to dissociation (before zero-point energy corrections are added) is currently found to be $12.15 \text{ kcal mol}^{-1}$ compared with the earlier value of $10.6 \text{ kcal mol}^{-1}$. Much of this difference can be attributed to the larger basis set employed in the CASSCF/CCI study, since the basis set used by Curtiss and co-workers did not contain f functions on nitrogen or d functions on hydrogen. The d and f functions, which describe higher angular momentum states, are essential to the calculation of an accurate D_e value for the HN_2 species.

As Table III. indicates, there are significant differences among the normal mode frequencies calculated in the current work and in that of Curtiss and co-workers. The values of ω_3 (primarily the HNN bending motion) computed in the two studies are in good agreement at both the HN_2 minimum and the saddle point of the $\text{H} + \text{N}_2$ potential energy surface. However, this is not true of the other two normal mode frequencies. The calculated values of ω_1 (primarily the NH stretching motion) and ω_2 (primarily the NN stretching motion) differ substantially at the stationary points. Further, while the study of Curtiss and co-workers reports a puzzling increase in the ω_2 frequency at both the saddle point and at the HN_2 minimum compared to its value in the N_2 molecule despite a lengthening of the NN bond, the ω_2 frequency

does not exhibit such anomalous behavior in the CASSCF/CCI calculations. In the current study, as the NN bond lengthens, the ω_2 frequency decreases monotonically. The unexplained behavior of the ω_2 frequency in the work of Curtiss et al. suggests a dramatic breakdown of the Møller-Plesset perturbation expansion. As noted above, this effect is not surprising since the N_2 triple bond requires a multireference description to correctly represent the elongation of the NN bond.

Finally, we determined the minimum energy path (MEP) for the addition of H atom to N_2 by computing a series of two-dimensional grids defined in terms of R_{NN} and θ (the HNN angle) for various values of R_{NH} ($R_{NH} = 4.5, 4.0, 3.5, 3.0, 2.8, 2.6, 2.4, 2.2, 2.0$, and $1.8 a_0$). A quadratic polynomial in R_{NN} and θ was then fitted to each of these calculated grids (using a linear least-squares procedure), and the minima of the resulting polynomials located. While all the computed energy values are contained in the appendix, Table IV. lists the coordinates, the corresponding potential energy values, and the normal mode frequencies orthogonal to the MEP (computed from the quadratic polynomials). Figure 1 depicts the energy along the MEP as a function of the R_{NH} distance. At large R_{NH} distances, the H atom initially approaches N_2 at an angle of $\approx 119^\circ$, with θ decreasing to $\approx 115^\circ$ as R_{NH} assumes its equilibrium value in HN_2 . Simultaneously, the NN bond gradually elongates as the R_{NH} distance decreases. These features of the MEP are similar to those observed in the addition of H atom to O_2 ⁴⁷.

IV. Dynamical Results

From the point of view of reaction dynamics, the lifetime of a species is perhaps the most elementary molecular property open to investigation. In the case of an extremely reactive intermediate, this parameter plays a crucial role in determining the ability of the species to participate in subsequent chemical reactions. We now

present a relatively straightforward, two-step analysis of the HN_2 lifetime, utilizing both Conventional Transition State Theory in its thermodynamic formulation, and an Eckart barrier formalism which estimates the role of one-dimensional quantum mechanical tunneling in the unimolecular decay process. This analysis uses information from the stationary points and the MEP of the molecular potential energy surface, but does not attempt to describe the microscopic details of the HN_2 decomposition process. An investigation of these details requires a more comprehensive representation of the potential energy surface and is left to future work. Rather, our intent is to obtain a new estimate of the HN_2 lifetime based on the current CASSCF/CCI calculations, to compare this estimate with a previous determination of the HN_2 lifetime, and to assess the implications of these lifetime estimates for the chemistry of the HN_2 species.

The upper portion of Table V. contains a summary of the thermodynamic properties of the $\text{H} + \text{N}_2 \rightarrow \text{HN}_2$ reaction based on information determined at the stationary points of the potential energy surface and calculated with statistical mechanics. This data is divided into two sections, the first reflects the changes in the thermodynamic state functions between the HN_2 minimum and the $\text{H} + \text{N}_2$ asymptote, while the second tabulates the same changes between the HN_2 minimum and the transition state (quantities marked by ‡). In both cases the HN_2 minimum has been chosen as the zero of energy. The data is from three distinct sources: (1) column one is based on the current CASSCF/CCI calculations using the [4s3p2d1f] basis set; (2) column two contains results from recent Bond Additivity Correction with fourth-order Møller-Plesset perturbation theory (BAC-MP4) calculations of Melius and Binkley⁴⁸; (3) the remaining columns summarize the results of the MP3/MP4 calculations of Curtiss and co-workers³⁵.

Before discussing the HN_2 lifetimes computed from the thermodynamic data us-

ing Conventional Transition State Theory, several characteristics of the data itself deserve comment. While columns three and four list the results reported by Curtiss et al. (Table 6. of reference 35.), columns five and six contain the same quantities calculated directly from the energetics, geometries, and frequencies of reference 35. In the first section of the data (relating changes between the HN_2 minimum and the $\text{H} + \text{N}_2$ asymptote), there are minor discrepancies (several tenths of a kcal mol^{-1}) between the reported and the calculated values of ΔH at both 0 K and 298.15 K. These differences arise from the apparent use by Curtiss and co-workers of both an N_2 frequency and bond length near the experimental values (2359 cm^{-1} and $2.075 a_0$) to prepare their reported data, compared with the MP3/6-31G** harmonic frequency of 2534 cm^{-1} and computed bond length of $2.090 a_0$ used to generate the corresponding calculated MP3/MP4 values. We have utilized the MP3/6-31G** harmonic frequency and bond length in preparing the calculated results to allow a more direct comparison with the thermodynamic quantities based on the CASSCF/CCI calculations. There is, however, a more serious discrepancy between the reported and calculated values of ΔS ; they differ in both magnitude and sign. While two different computational approaches have yielded consistent MP3/MP4 values of ΔS which agree with both the CASSCF/CCI and BAC-MP4 (computed independently) results, we have been unable to identify a reason for the differences observed in Table V. Since the a value of ΔS is not used in the Transition State Theory calculations of the HN_2 lifetime, the conclusions of Curtiss and co-workers are not affected by this apparent anomaly in the reported ΔS value. The remaining thermodynamic data of Table V. (relating changes between the HN_2 minimum and the transition state) exhibit some variations between the reported and calculated MP3/MP4 values which do affect the computed HN_2 lifetimes, but only in a relatively minor way. Again, the conclusions of Curtiss et al. are not

affected by these small changes.

The lower portion of Table V. summarizes the classical (that is, no quantum mechanical tunneling) HN_2 lifetimes computed with conventional Transition State Theory from the expression:

$$\tau = \left(\frac{h}{kT} \right) \exp \left(\frac{-\Delta S_T^{0\dagger}}{R} + \frac{\Delta H_T^{0\dagger}}{RT} \right) \quad (10)$$

where h is Planck's constant, k is Boltzmann's constant, R is the gas constant, and T is temperature (equation (10) is simply the reciprocal of the Transition State Theory rate coefficient for the unimolecular decay of HN_2). The values reported by Curtiss and co-workers are consistent with the calculated MP4 results listed in the Table, while the lifetimes predicted by the CASSCF/CCI data are approximately two orders of magnitude greater at 298.15 K and approximately 19 orders of magnitude greater at 30.0 K. These differences are a simple consequence of the disparate barriers to unimolecular decay predicted by the two sets of *ab initio* data. At this approximate level of theory it is inappropriate to attach significance to these differences or to the precise numerical values, and the general conclusions of the two studies, based on conventional Transition State Theory calculations, are the same. First, the lifetime of the HN_2 species at room temperature is very short (on the order of tenths to thousandths of a microsecond); secondly, at very low temperature, the predicted very long lifetime of HN_2 may permit experimental observation of the species.

Up to this point in our analysis, the HN_2 species has been treated in a purely classical manner, ignoring quantum mechanical effects. This approach has allowed a direct comparison with a portion of the study by Curtiss and co-workers. However, since the *ab initio* calculations discussed earlier indicate that the HN_2 minimum

lies at least 3 kcal mol⁻¹ above the H + N₂ asymptote, every rovibrational state supported by the HN₂ well is only quasi-bound. Consequently, quantum mechanical tunneling plays an essential role in the unimolecular decay of HN₂. Curtiss and co-workers accounted for these quantal effects by computing the tunneling frequency of a bound particle through a parabolic barrier. In this study we have used an Eckart function to model the vibrationally adiabatic barrier to HN₂ dissociation, computing HN₂ lifetimes based on an estimate of the one-dimensional quantal tunneling through that barrier. The vibrationally adiabatic potential was determined by adding the zero-point energy contribution of the NN stretching motion and the HNN bending motion (frequencies listed in Table IV.) to the computed potential energy along the MEP. Further, because all of the rovibrational states of the HN₂ species appear to be only quasi-bound, it does not seem appropriate to compute unimolecular lifetimes by assuming a thermally-averaged Boltzmann distribution (as does the thermodynamic formulation of Transition State Theory) created by multiple collisions of the HN₂ species with other molecules in the gas-phase. Instead, the formalism of W. H. Miller³⁹ was utilized to calculate unimolecular lifetimes as a function of the energy of each HN₂ quasi-bound vibrational state (microcanonical lifetimes). For the purposes of this study, we have assumed that J = 0 (that is, the HN₂ species is rotationally cold), although the formalism is not limited to this case alone.

Table VI. summarizes the calculated unimolecular lifetimes of HN₂ as a function of the energy of each quasi-bound vibrational state. In order to provide a careful estimate of the quantal tunneling effects, the calculations reported in Table VI. represent the results of three distinct Eckart Barrier models (designated Eckart Barrier-1, Eckart Barrier-2, and Eckart Barrier-3). In these models, the three parameters which completely determine the Eckart function, the height of the barrier

with respect to HN_2 (V_0), the height of the barrier with respect to $\text{H} + \text{N}_2$ (V_1), and the imaginary frequency (which determines the curvature at the top of the barrier) (ω^*), were systematically varied in an attempt to reflect accurately the properties of the HN_2 potential energy surface.

In the first model, Eckart Barrier-1, no effort was made to fit numerically the Eckart function to the shape of the vibrationally adiabatic potential. Rather, the parameters V_0 , V_1 , and ω^* were set equal to the zero-point-corrected (adding the zero-point energy of the NN stretch and the HNN bend) *ab initio* potential energy values and to the calculated imaginary frequency. Table VI. reports three calculations of the HN_2 lifetime as a function of energy using the Eckart Barrier-1 model: (1) a calculation using the *ab initio* results of the [4s3p2d1f] basis set, with $V_0 = 12.417 \text{ kcal mol}^{-1}$, $V_1 = 15.931 \text{ kcal mol}^{-1}$, and $\omega^* = 1662.2i \text{ cm}^{-1}$; (2) a calculation using the *ab initio* results of the [5s4p3d2f] basis set (at the [4s3p2d1f] geometry), with $V_0 = 11.549 \text{ kcal mol}^{-1}$, $V_1 = 15.777 \text{ kcal mol}^{-1}$, and $\omega^* = 1662.2i \text{ cm}^{-1}$; (3) a calculation using the MP4/6-31G** results of Curtiss and co-workers with $V_0 = 10.310 \text{ kcal mol}^{-1}$, $V_1 = 26.350 \text{ kcal mol}^{-1}$, and $\omega^* = 1533i \text{ cm}^{-1}$. Figure 2. compares the Eckart Barrier-1 model to the vibrationally adiabatic potential computed with the [4s3p2d1f] basis set. As Table VI. indicates, the MP4/6-31G** potential energy surface of Curtiss and co-workers supports only two quasi-bound vibrational states, while the potential energy surfaces computed in this work with the [4s3p2d1f] basis set and the [5s4p3d2f] basis set support six and five quasi-bound vibrational states, respectively. The Table also demonstrates the dynamical effect of using a larger *ab initio* basis set on the HN_2 lifetimes which range from 6.37×10^{-9} seconds to 1.76×10^{-13} seconds for the six vibrational levels of the [4s3p2d1f] basis, and from 1.25×10^{-9} seconds to 1.02×10^{-13} seconds for the five vibrational levels of the [5s4p3d2f] basis. Finally, the lifetime computed for HN_2

dissociation from the lowest vibrational state of the [4s3p2d1f] potential energy surface is approximately two orders of magnitude greater than the lifetime calculated for the unimolecular decay of HN_2 from the lowest vibrational state supported by the MP4/6-31G** potential energy surface.

However, as Figure 2. indicates, the Eckart Barrier-1 model both significantly overestimates the width of the barrier and does not closely approximate the shape of the vibrationally adiabatic potential. We therefore attempted to define a single model which is able to represent accurately both the width of the barrier and the shape of the vibrationally adiabatic potential. This proved to be impossible. Consequently, two additional models were constructed by numerically fitting (in a non-linear, least-squares sense) an Eckart function to the vibrationally adiabatic potential determined with the [4s3p2d1f] basis set. In the first of these new models, designated Eckart Barrier-2, V_0 was held fixed at the value used in the Eckart Barrier-1 model, while V_1 and ω^* were treated as adjustable parameters. The fitted Eckart Barrier-2 model is characterized by the parameters $V_0 = 12.417 \text{ kcal mol}^{-1}$, $V_1 = 12.997 \text{ kcal mol}^{-1}$, and $\omega^* = 2441.3i \text{ cm}^{-1}$, but, as Figure 3. indicates, it significantly underestimates the width of the barrier. This model does, however, possess the attribute of closely approximating the shape of the HN_2 side of the vibrationally adiabatic potential. The second of the new models, identified as Eckart Barrier-3, was constructed by holding both V_0 and V_1 fixed at the values which characterize the Eckart Barrier-2 model (hence, V_0 is the same value in all three models considered in this work) and treating ω^* as the only adjustable parameter in the non-linear least-squares fitting procedure. The resulting Eckart Barrier-3 model is defined by the parameters $V_0 = 12.417 \text{ kcal mol}^{-1}$, $V_1 = 12.997 \text{ kcal mol}^{-1}$, and $\omega^* = 1715.6i \text{ cm}^{-1}$, and is compared in Figure 4. to the vibrationally adiabatic potential. While the Eckart Barrier-3 model overestimates the width of

the barrier, it does succeed in closely approximating the shape of $\text{H} + \text{N}_2$ side of the vibrationally adiabatic potential.

The two models provide a lower bound (Eckart Barrier-2) and an upper bound (Eckart Barrier-3) for the HN_2 unimolecular lifetime of each quasi-bound vibrational state associated with the $[4s3p2d1f]$ basis set. These bounds are summarized in the final two columns of Table VI. Note that as the top of the barrier is approached, the widths of the two model barriers become increasingly similar. Consequently, the difference between the two lifetimes computed for each quasi-bound vibrational state decreases with increasing energy. In the case of the lowest-lying quasi-bound vibrational state, the two computed lifetimes differ by approximately a factor of 66; for the highest-lying state, they differ only by approximately a factor of 1.4. The HN_2 lifetimes predicted by these two models, which include the effects of quantum mechanical tunneling, suggest that the HN_2 species is extremely short-lived, even at very low temperatures. As a result, we expect that it will be difficult to observe the HN_2 species experimentally, and that the role of HN_2 in both termolecular recombination processes and combustion processes will be dramatically limited by its very short lifetime.

V. Conclusions

This study has focused on two aspects of the addition of atomic hydrogen to N_2 : first, a characterization of the minimum energy path for the addition reaction, and secondly, a determination of the unimolecular lifetime of the HN_2 species. While this work has presented neither a global description of the potential energy surface for the addition reaction nor a discussion of the microscopic details of the dynamics, it has reached several important conclusions:

- (1) The HN_2 minimum is found to lie approximately $3.01 \text{ kcal mol}^{-1}$ above the

H + N₂ asymptote, compared to 14.4 kcal mol⁻¹ calculated earlier by Curtiss and co-workers.

- (2) While this earlier study computed a zero-point-corrected barrier to dissociation of approximately 5.8 kcal mol⁻¹, the current work has estimated this barrier to be approximately 8.5 kcal mol⁻¹.
- (3) The current calculations indicate that six quasi-bound vibrational levels exist in the HN₂ well, compared to the two quasi-bound levels predicted in the earlier study of Curtiss and co-workers.
- (4) The current work has used both a larger basis set and an improved methodology to calculate a new estimate of the NN harmonic stretching frequency in the N₂ and HN₂ species.
- (5) We estimate that the lifetime of the lowest-lying quasi-bound vibrational state of HN₂ to lie between 8.8×10^{-11} seconds and 5.8×10^{-9} seconds. This predicted lifetime is between a factor of two and a factor of one hundred longer than the lifetime of the HN₂ species predicted by Curtiss and co-workers.
- (6) However, we conclude, in concert with the conclusions of Curtiss and co-workers, that it will be very difficult to observe the HN₂ species experimentally, and that the predicted short lifetime of the HN₂ species will severely circumscribe its role in both termolecular reaction mechanisms and proposed combustion mechanisms.

ACKNOWLEDGEMENTS

S. P. Walch and R. J. Duchovic gratefully acknowledge the support of NASA grants NCC 2-478 and NCC 2-512, respectively. Special thanks to Dr. David Schwenke (ELORET Institute), Dr. Carl Melius (Sandia National Laboratory), and Dr. James Miller (Combustion Research Facility) for helpful discussions.

REFERENCES

1. J. A. Logan, M. J. Prather, S. C. Wofsy, and M. B. McElroy, *J. Geophys. Res.*, **86**, 7210(1981).
2. W. C. Gardiner, Jr. and D. B. Olson, *Ann. Rev. Phys. Chem.*, **31**, 377(1980).
3. P. G. Glarborg, J. A. Miller, and R. J. Kee, *Combustion and Flame*, **65**, 177(1986).
4. J. A. Miller, M. C. Branch, and R. J. Kee, *Combustion and Flame*, **43**, 81(1981).
5. S. Salimian and R. K. Hanson, *Combustion Science and Technology*, **23**, 225(1980).
6. C. M. Bamford, *Trans. Faraday Soc.*, **35**, 568(1939).
7. A. Serewicz and W. A. Noyes, Jr., *J. Phys. Chem.*, **63**, 843(1959).
8. R. Srinivasan, *J. Phys. Chem.*, **64**, 679(1960).
9. C. P. Fenimore and G. W. Jones, *J. Phys. Chem.*, **65**, 298(1961).
10. S. Gordon, W. Mulac, and P. Nangia, *J. Phys. Chem.*, **75**, 2087(1971).
11. M. Gehring, K. Hoyer mann, H. Schacke, and J. Wolfrum, Fourteenth Symposium (International) on Combustion, The Combustion Institute, 1972, p. 99.
12. W. E. Kaskan and D. E. Hughes, *Combustion and Flame*, **20**, 381(1973).
13. R. Lesclaux, P. V. Khe, P. Dezaudier, and J. C. Soullignac, *Chem. Phys. Lett.*, **35**, 493(1975).
14. G. Hancock, W. Lange, M. Lenzi, and K. H. Welge, *Chem. Phys. Lett.*, **33**, 168(1975).
15. W. Hack, H. Schacke, M. Schroeter, and Gg. Wagner, Seventeenth Symposium

- (International) on Combustion, The Combustion Institute, 1978, p. 505.
16. J. A. Silver, C. M. Gozewski, and C. E. Kolb, Aerodyne Research Inc. Report, **ARI-RR-235**, November, 1980.
 17. J. A. Silver and C. E. Kolb, J. Phys. Chem., **86**, 3240(1982).
 18. L. J. Steif, W. D. Brobst, D. F. Nava, R. P. Borkowski, and J. V. Michael, Faraday Trans. 2, **78**, 1391(1982).
 19. A. M. Dean, J. E. Hardy, and R. K. Lyon, Nineteenth Symposium (International) on Combustion, The Combustion Institute, 1982, p. 97.
 20. P. Andresen, A. Jacobs, C. Kleinermanns, and J. Wolfrum, Nineteenth Symposium (International) on Combustion, The Combustion Institute, 1982, p. 11.
 21. A. R. Whyte and L. F. Phillips, Chem. Phys. Lett., **102**, 451(1983).
 22. J. P. Seidle and M. C. Branch, Combustion and Flame, **52**, 47(1983).
 23. A. R. Whyte and L. F. Phillips, J. Phys. Chem., **88**, 5670(1984).
 24. T. Drier and J. Wolfrum, Twentieth Symposium (International) on Combustion, The Combustion Institute, 1984, p. 695.
 25. A. M. Dean, M.-S. Chou, and D. Stern, Int. J. Chem. Kinet., **16**, 633(1984).
 26. C. J. Dasch and R. J. Blint, Combustion Science and Technology, **41**, 223(1984).
 27. M. A. Kimball-Linne and R. K. Hanson, Combustion and Flame, **64**, 337(1986).
 28. J. L. Hall, D. Zeitz, J. W. Stephens, J. V. V. Kasper, G. P. Glass, R. F. Curl, and F. K. Tittel, J. Phys. Chem., **90**, 2501(1986).
 29. D. A. Dolson, J. Phys. Chem., **90**, 6714(1986).
 30. W. A. Lathan, L. A. Curtiss, W. J. Hehre, J. B. Lisle, and J. A. Pople, Progr. Phys. Org. Chem., **11**, 175(1974).

31. K. Vasudevan, S. D. Peyerimhoff, and R. J. Buenker, *J. Mol. Struct.*, **29**, 285(1975).
32. N. C. Baird, *J. Chem. Phys.*, **62**,300(1975).
33. N. C. Baird and H. B. Kathpal, *Can. J. Chem.*, **55**, 863(1977).
34. C. J. Casewit and W. A. Goddard, III, *J. Am. Chem. Soc.*, **102**, 4057(1980).
35. L. A. Curtiss, D. L. Drapcho, and J. A. Pople, *Chem. Phys. Lett.*, **103**, 437(1984).
36. P. E. M. Siegbahn, *Int. J. Quantum Chem.*, **23**, 1869(1983).
37. J. Almlöf and P. R. Taylor, *J. Chem. Phys.*, **86**, 4070(1987).
38. For recent reviews of Transition State Theory see D. G. Truhlar, W. L. Hase, and J. T. Hynes, *J. Phys. Chem.*, **87**, 2664(1983) and D. G. Truhlar, A. D. Isaacson, and B. C. Garrett in: "Theory of Chemical Reaction Dynamics", Vol. 4, ed. M. Baer, (CRC Press, Boca Raton, FL, 1985), p. 65.
39. W. H. Miller, *J. Am. Chem. Soc.*, **101**, 6810(1979).
40. S. R. Langhoff and E. R. Davidson, *Int. J. Quant. Chem.*, **8**, 61(1974).
41. J. Almlöf, MOLECULE, a vectorized Gaussian integral program.
42. SWEDEN is a vectorized SCF-MCSCF-direct CI, conventional CI-CPF-MCPF program written by P. E. M. Siegbahn, C. W. Bauschlicher, Jr., B. Roos, P. R. Taylor, A. Heiberg, J. Almlöf, S. R. Langhoff, and D. P. Chong.
43. K. Huber and G. Herzberg, "Molecular Spectra and Molecular Structure, Constants of Diatomic Molecules" Vol. 4., (Van Nostrand, Princeton, NJ, 1979).
44. S. P. Walch and R. L. Jaffe, *J. Chem. Phys.*, **86**, 6946(1987).
45. R. J. Bartlett and G. D. Purvis, III, *Phys. Scr.*, **21**, 255(1980).
46. W. D. Laidig, P. Saxe, and R. J. Bartlett, *J. Chem. Phys.*, **86**, 887(1987).
47. S. P. Walch, C. M. Rohlfing, C. F. Melius, and C. W. Bauschlicher, *J. Chem. Phys.*, **88**, 6273(1988).

48. C. F. Melius and J. S. Binkley, Twentieth Symposium (International) on Combustion, The Combustion Institute, 1984, p. 575.

Table I. Qualitative Character of the CASSCF Orbitals for $\text{H} + \text{N}_2 \rightarrow \text{HN}_2^+$

orbital	$\text{H} + \text{N}_2$	HN_2
1a'	N1s	N1s
2a'	N1s	N1s
3a'	N2s	N2s
4a'	N2s	N2s
5a'	$\text{N}_2 3\sigma_g$	$\text{N}_2 3\sigma_g$
6a'	$\text{N}_2 1\pi_u$	$\text{N}_2 1\pi_u + \text{H}1s$
7a'	H1s	$\text{N}_2 1\pi_g + \text{H}1s$
8a'	$\text{N}_2 1\pi_g$	$\text{N}_2 1\pi_g - \text{H}1s$
9a'	$\text{N}_2 3\sigma_u$	$\text{N}_2 3\sigma_u$
1a''	$\text{N}_2 1\pi_u$	$\text{N}_2 1\pi_u$
2a''	$\text{N}_2 1\pi_g$	$\text{N}_2 1\pi_g$

Table II. Computed Potential Curve Parameters for N₂.

	[4s3p2d1f] basis	[5s4p3d2f] basis	[5s4p3d2f1g] basis	Exp.
R _e	2.096		2.089	2.074
ω _e	2286		2269	2359
D ₀	212	217	219	225.0

R_e in a₀, ω_e in cm⁻¹, D₀ in kcal mol⁻¹

Table III. Stationary Points on the H + N₂ Surface.^a

	this work			CDP ^b		
	H + N ₂ minimum	H—N ₂ saddle point	HN ₂ minimum	H + N ₂ minimum	H—N ₂ saddle point	HN ₂ minimum
R _{NH}	20.0	2.753	2.007		2.670	1.975
R _{NN}	2.095	2.146	2.262	2.090	2.101	2.186
θ		118.6	116.3		119.9	118.0
ω_1		1662i	2744		1533i	3077
ω_2	2303	2072	1583	2534	2743	2619
ω_3		771	1070		766	1079
ΔE^c	-3.01	12.15	0.0	-14.4 ^d	10.6 ^d	0.0 ^d
ZPE ^e	3.29	4.06	7.72			
$\Delta E_{corr.}$	-7.44	8.49	0.0			

^a Energies are in kcal mol⁻¹, bond lengths in a₀, angles in degrees, and vibrational frequencies are in cm⁻¹. This work used the [4s3p2d1f/3s2p1d] basis set.

^b Curtiss, Drapcho, and Pople, reference 35.

^c Energy relative to HN₂.

^d Based on MP4/6-31G** energies evaluated at MP3/6-31G** geometries.

^e Zero-Point Energy

Table IV. Computed Minimum Energy Path for $\text{H} + \text{N}_2$.^a

R_{NH}	R_{NN}	θ	ω_2	ω_3	$E(\text{CCI} + Q)$ (hartree)	ΔE^b (kcal mol ⁻¹)
20.0	2.095		2303		-109.88077	-3.01
4.5	2.096	118.8	2286	112	-109.87808	-1.33
4.0	2.097	119.5	2285	187	-109.87457	0.88
3.5	2.101	119.4	2278	315	-109.86801	5.00
3.0	2.118	119.2	2245	550	-109.85911	10.58
2.8	2.133	119.0	2218	680	-109.85699	11.91
2.6	2.172	117.0	1968	849	-109.85769	11.47
2.4	2.205	116.2	1193	969	-109.86352	7.81
2.2	2.232	116.1	1886	1026	-109.87121	2.99
2.0	2.278	114.7	1566	899	-109.87579	0.11
1.8	2.255	117.6	1202	1659	-109.87078	3.25

^a Bond lengths are in a_0 , angles are in degrees, and frequencies in cm^{-1} .

^b Energy relative to HN_2 minimum.

Table V. Thermodynamic Properties and Unimolecular Lifetimes for $\text{HN}_2 \rightarrow \text{H} + \text{N}_2$

Thermodynamic Data						
	CASSCF	BAC-MP4 ^a	MP3 (reported ^b)	MP4	MP3 (calculated ^c)	MP4
ΔE	-3.0129	-	-10.3	-14.4	-10.2785	-14.3762
ΔH_0^0	-7.4362	-8.0	-16.6	-20.7	-16.3414	-20.4390
ΔH_{298}^0	-6.2709	-6.8	-15.4	-19.5	-15.1734	-19.2710
ΔS_{298}^0	19.4687	19.8	-2.78	-2.78	19.6605	19.6605
ΔE^\ddagger	12.1450	-	13.5	10.5	13.5102	10.5978
ΔH_0^\ddagger	8.4947	6.3	8.8	5.8	8.8412	5.9108
ΔH_{30}^\ddagger	8.4947	-	-	-	8.8412	5.9108
ΔH_{298}^\ddagger	8.5298	6.3	8.9	5.9	8.8799	5.9495
ΔS_{30}^\ddagger	0.4924	-	-	-	0.5154	0.5154
ΔS_{298}^\ddagger	0.6466	0.6708	0.72	0.72	0.6834	0.6834
Lifetimes						
Temp	CASSCF	CDP (reported ^b)	MP3 (calculated ^c)	MP4		
30.0 K	9.53×10^{49}	1.1×10^{31}	3.16×10^{52}	1.42×10^{31}		
298.15 K	2.08×10^{-7}	2.2×10^{-9}	3.69×10^{-7}	2.62×10^{-9}		

^a Melius and Binkley, reference 48.^b Curtiss, Drapcho, and Pople, reference 35.^c See text.

† Refers to thermodynamic quantities of the transition state; remaining thermodynamic quantities are those of the $\text{H} + \text{N}_2$ asymptote. Both sets of thermodynamic data are calculated with respect to the HN_2 minimum. Energies and enthalpies are in kcal mol^{-1} , entropies in $\text{cal mol}^{-1} \text{ deg}^{-1}$, and lifetimes in seconds.

Table VI. Calculated Unimolecular Lifetimes^a of IIN₂

Quasi-Bound State ^b	this work		
	Eckart Barrier-1 [4s3p2d1f]	[5s4p3d2f]	Eckart Barrier-2 [4s3p2d1f]
7.72	6.37×10^{-9}	1.25×10^{-9}	8.82×10^{-11}
10.78	5.95×10^{-11}	1.46×10^{-11}	4.30×10^{-12}
12.24	7.95×10^{-12}	2.14×10^{-12}	1.19×10^{-12}
13.84	1.04×10^{-12}	3.30×10^{-13}	3.42×10^{-13}
15.30	2.18×10^{-13}	1.02×10^{-13}	1.40×10^{-13}
15.56	1.76×10^{-13}	—	1.24×10^{-13}

CDP ^c	
Quasi-Bound State ^b	Eckart Barrier-1 [MP4/6-31G**]
9.69	7.13×10^{-11}
12.77	8.60×10^{-13}

^a Lifetimes in seconds.

^b Energies of quasi-bound states in kcal mol⁻¹.

^c Curtiss, Drapcho, and Pople, reference 35.

FIGURE CAPTIONS

Figure 1.: Interaction energy for the addition of a hydrogen atom to N_2 as a function of R_{NH} along a minimum energy path (MEP) obtained by optimizing R_{NN} and θ at each R_{NH} value. The energies are from CASSCF/CCI + Q calculations (see text).

Figure 2.: Eckart Barrier-1 model. The bold solid curve is the vibrationally adiabatic barrier calculated from the CASSCF/CCI + Q data along the minimum energy path (MEP). The solid curve is an Eckart function. The horizontal dashed curves represent the quasi-bound vibrational states of the HN_2 well. In the separable harmonic approximation, the energy of each vibrational state is given by $E_{(n_1, n_2, n_3)} = \sum_{i=1}^3 (n_i + \frac{1}{2})h\nu_i$. Each state is identified by a set of quantum numbers (n_1, n_2, n_3) , where $n_1 = HN \text{ stretch}$ quantum number, $n_2 = NN \text{ stretch}$ quantum number, $n_3 = HNN \text{ bend}$ quantum number.

Figure 3.: Eckart Barrier-2 model. The bold solid curve is the vibrationally adiabatic barrier calculated from the CASSCF/CCI + Q data along the minimum energy path (MEP). The solid curve is an Eckart function. The horizontal dashed curves represent the quasi-bound vibrational states of the HN_2 well. In the separable harmonic approximation, the energy of each vibrational state is given by $E_{(n_1, n_2, n_3)} = \sum_{i=1}^3 (n_i + \frac{1}{2})h\nu_i$. Each state is identified by a set of quantum numbers (n_1, n_2, n_3) , where $n_1 = HN \text{ stretch}$ quantum number, $n_2 = NN \text{ stretch}$ quantum number, $n_3 = HNN \text{ bend}$ quantum number.

Figure 4.: Eckart Barrier-3 model. The bold solid curve is the vibrationally adiabatic barrier calculated from the CASSCF/CCI + Q data along the minimum energy path (MEP). The solid curve is an Eckart function. The horizontal dashed curves represent the quasi-bound vibrational states of the HN_2 well. In the separable harmonic approximation, the energy of each vibrational state is given by $E_{(n_1, n_2, n_3)} = \sum_{i=1}^3 (n_i + \frac{1}{2})h\nu_i$. Each state is identified by a set of quantum numbers (n_1, n_2, n_3) , where $n_1 = HN \text{ stretch}$ quantum number, $n_2 = NN \text{ stretch}$ quantum number, $n_3 = HNN \text{ bend}$ quantum number.

